Elastic and optical properties of α- and κ-Al$_2$O$_3$

B. Holm

Department of Applied Physics, Chalmers University of Technology and Göteborg University, S-412 96 Göteborg, Sweden

R. Ahuja

Condensed Matter Theory Group, Department of Physics, Uppsala University, Box 530, S-751 21 Uppsala, Sweden

Y. Yourdshahyan

Department of Applied Physics, Chalmers University of Technology and Göteborg University, S-412 96 Göteborg, Sweden

B. Johansson

Condensed Matter Theory Group, Department of Physics, Uppsala University, Box 530, S-751 21 Uppsala, Sweden

B. I. Lundqvist

Department of Applied Physics, Chalmers University of Technology and Göteborg University, S-412 96 Göteborg, Sweden

We present theoretical results for various properties of the stable α and metastable κ phase of alumina, in particular elastic and optical properties. Two different computational methods have been used, the dacapo plane-wave-pseudopotential and the full potential linearized muffin tin orbital methods. The calculations are based upon a recent determination of the crystal structure of κ-Al$_2$O$_3$. Comparison between the two methods and available experimental data show that they are both reliable for calculating the ground-state and mechanical properties for this type of complex material. [S0163-1829(99)09519-3]

I. INTRODUCTION

Aluminum oxide (alumina) is a ceramic material of great interest both for applications and fundamental studies. Alumina is also fascinating from the point of view that it can appear in many different phases. During the last few decades the stable α phase (corundum) has undergone thorough experimental and theoretical investigations. A review of its properties is given by French.[1] The material is highly insulating, characterized by mixed ionic and covalent bonding. It is also very hard and wear resistant. Recent developments of industrial applications of alumina have directed interest to other, metastable, phases of alumina, in particular the so-called γ and κ phases. The complicated crystal structure in these cases has provided both experimentalists and theoreticians with different, nontrivial challenges. As for the experimental situation, one of the main obstacles for deeper studies of the properties of the various phases of alumina consists of the difficulty in producing a significant amount of a sample that is pure and homogeneous, i.e., without distortions, grain boundaries, etc. On the theoretical side, the complexity of the crystal structure of this material has prevented its understanding on a first-principle level. Instead, approximations and phenomenological theories with empirical parameters had to be relied upon in the investigations of ground-state, mechanical, optical, and other properties. However, with the increase of computer speed and power, alumina has become accessible for *ab initio* studies. Hence, there have been results presented from such studies of bulk[2] and surface[3] α-Al$_2$O$_3$, as well as for the important case of impurities in this system.[4]

The task of determining the positions of the constituent atoms in κ-Al$_2$O$_3$ has not been solved until recently[5,6] (1997), and in this paper, we present some results that follow from a knowledge of the crystal structure of kappa alumina.

We especially focus on the differences and similarities between the κ and α phases.

In general, the complicated bulk structure of the different phases of alumina can be viewed upon as close-packed stacking sequences of oxygen with aluminum atoms occupying octahedral and/or tetrahedral interstices.

The α-Al$_2$O$_3$ unit cell can be described as hexagonal or rhombohedral, depending on the crystallographical definition of the space group $R\bar{3}_c$. The crystal structure[7] consists of O atoms in a close-packed hexagonal array with Al atoms occupying two-thirds of the octahedral interstitial sites. The oxygen layers are in an $ABABAB$ stacking sequence, where each O atom is bonded to four Al atoms in a distorted sp^3 arrangement, while the Al atoms are bonded to six nearest-neighbor oxygen atoms. There are two nearest-neighbor bond lengths, 1.86 Å and 1.96 Å .

The crystal structure of the κ-Al$_2$O$_3$ unit cell belongs to the orthorhombic class with point group $mm2$ and space group $Pna2_1$, containing eight molecular units per cell. The unit cell consists of four close-packed oxygen layers in an $ABAC$ stacking sequence along the **c** axis and Al atoms occupying both octahedral and tetrahedral interstitial positions. The Al ions can be arranged in six layers. Each of the Al layers situated between the B and A and between the C and A oxygen layers consists of four Al atoms occupying octahedral sites. The remaining four Al planes consist of two Al atoms each, where the Al atoms in two layers occupy tetrahedral positions, the other two occupy octahedral ones. One of each type of plane will be in between the rest of the oxygen layers (see Fig. 1).

Elastic constants of materials describe physical properties of importance beyond the macroscopic elastic behavior of the material. For instance, elastic aspects of dislocations and dislocation interactions are accounted for, and fracture
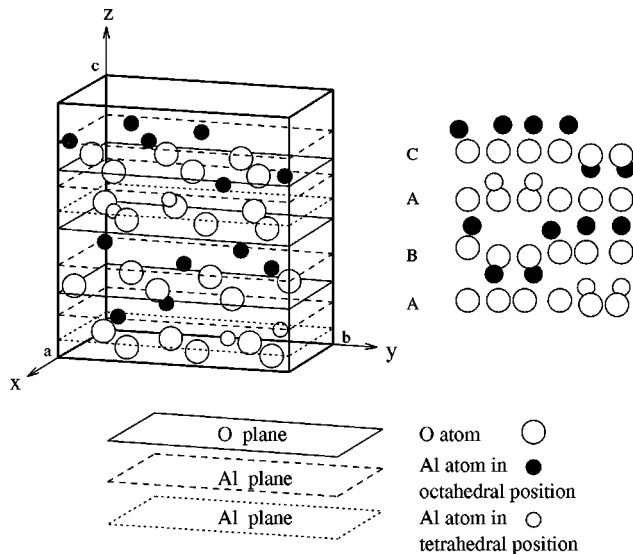
FIG. 1. Crystal structure of κ alumina in three and two dimensions. Capital letters denote oxygen stacking layers and small letters the aluminum ones.

toughness can be calculated using linear fracture mechanics. Elastic constants are also a measure of the strength of the forces between the atoms. From a geophysical point of view, the study of the elastic properties of Al_2O_3 is important for the understanding of the elastic behavior of the earth's lower mantle. Al_2O_3 is also used as an example of the applicability of the classical elastic theory to trigonal crystals. Consequently, there are a lot of experimental data available about the elastic constants of α-Al_2O_3.

Gieske and Barsch[8] have measured the six single-crystal elastic constants of Al_2O_3, using the ultrasonic pulse superposition method as a function of hydrostatic pressure up to 10 kbar. They found a linear pressure dependence for all six elastic constants. Tefft[9] reported the temperature dependence of the elastic constants of α-Al_2O_3, using a resonance technique in the temperature range of 80–900 K. Goto *et al.*[10] measured the elastic constants of single-crystal α-Al_2O_3 up to 1825 K using the rectangular parallelepiped resonance method. They have demonstrated that the elastic stiffness constants c_{11} and c_{33} show a large decrease, while c_{12} and c_{13} show only a slight decrease with temperature. The c_{44} decreases linearly with temperature whereas c_{14} is almost constant in the measured temperature range. Recently, Zouboulis and Grimsditch[11] measured the elastic constants c_{11}, c_{33}, and c_{44} using Brillouin scattering in the temperature range 300–2100 K, extending by 300 K the highest temperature previously attained.

Although electronic structure calculations have recently been performed for α-Al_2O_3, there is only one case that has been applied to the calculation of the elastic constants.[12] There, full potential linear combination of Gaussian-type orbitals–fitting function (LCGTOFF) technique was used to obtain the equation of state and elastic constants of corundum. Only the symmetry-preserving elastic constants, i.e., $c_{11}+c_{12}$, c_{33} and c_{13}, out of six elastic constants were calculated. As far as other recent electronic structure calculations[2] of α-Al_2O_3 are concerned, they are limited to the calculation of the lattice parameters, bulk modulus, and equation of state (EOS).

The dielectric function is a key quantity for the study of the optical properties of a material. Accurate knowledge of the dielectric functions over a wide range of wavelengths is indispensable for many applications. There is a continued experimental effort to study the optical properties of Al_2O_3. Recently, Harman *et al.*[13] measured the optical constants of α-Al_2O_3 using spectroscopic ellipsometry in the near-infrared–near-ultraviolet spectral region (1.2–5.4 eV) at room temperature. They used their own data as well as data available in the literature for modeling of the optical constants over the 0–30 eV energy range. Tomiki *et al.*[14] reported the optical constants of α-Al_2O_3 at 297 and 10 K over the range of photon energies 6–120 eV.

Zouboulis and Grimsditch[11] have shown that Brillouin scattering can be used to measure the elastic and optical properties of materials. They have demonstrated the temperature dependence of the ordinary and extraordinary refractive indices. Bortz and French[15] performed optical reflectivity measurements on a single crystal of α-Al_2O_3 from 5 to 40 eV using light produced by a laser plasma light source (LPLS). This was the first application, to our knowledge, of LPLS to vacuum ultraviolet spectroscopy of solids.

In the late 1970s, Arakawa and Williams[16] presented absorption data on anodized Al_2O_3 films for incident photon energies from 5 to 18 eV. From their measured transmittance and reflectance data of single-crystal Al_2O_3, they have derived the optical constants, dielectric constants, and energy-loss functions over the energy range 8–28.5 eV. They have interpreted their data in terms of excitons, interband transitions, and collective oscillations.

In spite of the availability of such a vast amount of experimental data, there has been no serious attempt to study the optical properties theoretically with *ab initio* methods. There is only one first-principles calculation available for the optical properties of α-Al_2O_3. Ching and Xu[17] studied the electronic and optical properties using an orthogonalized (frozen-core) linear combination of atomic orbitals (OLCAO) method in local-density approximation (LDA). In these calculations, no detailed comparison has been made between experiment and theory.

The main aim of this paper is to present *ab initio* calculations of the elastic and optical properties of the κ phase, as well as to provide additional data for the α phase, as an improvement over the calculations available in the literature. The paper is organized in the following way. In Sec. II, we give a brief review of the methods of calculation. Section III is devoted to the discussion of the electronic structure, optical response, and elastic properties. Finally, Sec. IV summarizes our results.

II. THEORETICAL BACKGROUND

The rapid development of theoretical methods and increase of computer capacity during the past years has made ''computational experiments'' possible for more and more complex materials. Our calculations use two different approaches—the plane-wave pseudopotential method (PWPP) (Ref. 18) and the full potential linear muffin-tin orbital method (FPLMTO).[19] This enables us to compare the performance of the former method with that of the latter, which can be considered more accurate as it does not depend

upon the typical pseudo-potential approximations.[20] Both methods rely upon density-functional theory (DFT),[21–23] but while the PWPP method provides wave functions for the valence electrons only, the FPLMTO one takes the core electrons into account as well, thus naturally demanding a much more substantial computer effort.

The general background to DFT is well described in, e.g., the original papers[21,22] and more recent reviews.[24,25] In the used dacapo program package,[26] as in all PWPP methods, the interaction of the valence electrons with the atomic cores is represented by pseudopotentials. The pseudopotentials used for oxygen and aluminum are the norm-conserving potentials of Troullier and Martins[27] and Bachelet *et al.*,[28] respectively. The one-electron wave functions are expanded in a plane-wave basis with a cutoff energy of 650 eV. To reduce the number of k points needed we use a finite electronic temperature of 0.1 eV, when determining the occupation numbers, and then extrapolate all total energies to zero electronic temperature.[29] In the self-consistent iterations, eight k points in a Monkhorst-Pack[30] sampling are used. This is deemed adequate for the κ-Al$_2$O$_3$ crystal.[31] The exchange and correlation energy is treated self-consistently within the local-density approximation,[32,33] and non-self-consistently in the generalized-gradient approximation (GGA), so-called post-GGA,[34,35] respectively, depending on the purpose of the calculation.

The FPLMTO method[19] solves a Dirac (for the core electrons) and a (modified) Schrödinger equation (for the valence and semicore electrons). The total energy of the system is again obtained within the LDA, for which the Hedin-Lundqvist[36] parametrization is used. The wave functions are expanded by means of linear muffin-tin orbitals inside the nonoverlapping muffin-tin spheres that surround each atomic site in the crystal.[37,38] The muffin-tin radius is consistently chosen such that the muffin-tin spheres occupy 66% of the total volume. A so-called double basis set, which allows two tails with different kinetic energies for each muffin-tin orbital with a given l-quantum number, has been used.

The calculations are performed for one fully hybridizing energy panel, in which we use values for the E_ν's related to the valence orbitals: $3s$, $3p$, and $3d$ for Al and $2s$, $2p$, and $3d$ for O. Within the muffin-tin spheres the basis set, charge density, and potential are expanded in spherical harmonics with a cutoff of $l_{max}=6$. Outside the muffin-tin spheres, in the interstitial region, the wave functions are Hankel or Neumann functions, which are represented by a Fourier series using reciprocal-lattice vectors. The same expansion is used to represent the charge density and the potential. This treatment of the wave functions, charge density, and potential does not rely upon any geometrical approximations.

A. Calculation of dielectric function

The ($q=0$) dielectric function is calculated in the momentum representation, using the FPLMTO result of our electron structure calculation. This requires matrix elements of the momentum, $\mathbf{p}$, between occupied and unoccupied eigenstates. To be specific, the imaginary part of the dielectric function, $\epsilon_2(\omega)\equiv\mathrm{Im}\,\epsilon(\mathbf{q}=0,\omega)$, is calculated from[39]

$$\epsilon_2^{ij}(\omega)=\frac{4\pi^2e^2}{\Omega m^2\omega^2}\sum_{\mathbf{k}nn'\sigma}\langle\mathbf{k}n\sigma|p_i|\mathbf{k}n'\sigma\rangle\langle\mathbf{k}n'\sigma|p_j|\mathbf{k}n\sigma\rangle$$

$$\times f_{\mathbf{k}n}(1-f_{\mathbf{k}n'})\delta(e_{\mathbf{k}n'}-e_{\mathbf{k}n}-\hbar\omega). \quad (1)$$

In Eq. (1), e is the electron charge, m its mass, Ω is the volume of the unit cell, and $f_{\mathbf{k}n}$ is the Fermi distribution. Moreover, $|\mathbf{k}n\sigma\rangle$ is the crystal wave function corresponding to the nth eigenvalue with crystal momentum $\mathbf{k}$ and spin σ.

With our spherical wave basis functions, the matrix elements of the momentum operator are conveniently calculated in spherical coordinates and for this reason the momentum is written $\mathbf{p}=\Sigma_\mu\mathbf{e}_\mu^*p_\mu$,[40] where μ is -1, 0, or 1, and $p_{-1}=(1/\sqrt{2})(p_x-ip_y)$, $p_0=p_z$, and $p_1=(-1/\sqrt{2})(p_x+ip_y)$.[41]

The evaluation of the matrix elements in Eq. (1) is done over the muffin-tin region and the interstitial one separately. The integration over the muffin-tin spheres is done in a way similar to what Khan,[42] Oppeneer,[43] and Gasche[39] have done in their calculations using the atomic-sphere approximation. A full and detailed description of the calculation of the matrix elements is presented in Ref. 44. The summation over the Brillouin zone in Eq. (1) is performed using a linear interpolation on a mesh of uniformly distributed points, i.e., the tetrahedron method. Matrix elements, eigenvalues, and eigenvectors are calculated in the irreducible part of the Brillouin zone. The correct symmetry for the dielectric constant was obtained by averaging the calculated dielectric function. Finally, the real part of the dielectric function, $\epsilon_1(\omega)$, is obtained from $\epsilon_2(\omega)$ using the Kramers-Kronig transformation,

$$\epsilon_1(\omega)\equiv\mathrm{Re}[\epsilon(\mathbf{q}=0,\omega)]$$

$$=1+\frac{1}{\pi}\int_0^\infty d\omega'\,\epsilon_2(\omega')\left(\frac{1}{\omega'-\omega}+\frac{1}{\omega'+\omega}\right). \quad (2)$$

For all our calculations of optical properties, the irreducible Brillouin zone has been sampled by 360 k points for the α phase and 240 for the κ phase. In order to speed up convergence, we have associated each eigenvalue with a Gaussian broadening of 270 meV.

B. Calculation of elastic constants for single-crystal and polycrystalline aggregates

The crystal structure of the κ phase is orthorhombic and that of the α phase is trigonal. The respective symmetries imply that there are nine independent elastic moduli for the κ phase and six for the α phase to be determined. Using the α phase as a point of reference, we conclude that the PWPP method is ample for this type of calculation. Furthermore, as we are concerned with energy differences only, the LDA is sufficient for good results. This fact has been observed in similar situations.[4,45] Thus, the LDA has been used throughout the calculation of elastic constants.

The calculations are made by analyzing the energetic behavior of the crystal when applying small strains (this was accomplished by varying the primitive vectors of the unit cell). As the strains couple to the vibrational modes, the atoms have to be relaxed for each variation of the unit cell when performing the total-energy calculations, as was done by Karki *et al.*[46] To guide the reader, we show how the elas-

tic constants for the κ phase were obtained. The ones for the α phase are obtained in a similar manner, but in accordance with its symmetry.

From the theory of elasticity, the change of energy per unit volume in the crystal, when the vectors of the unit cell are being altered, is given by

$$\delta U = \frac{1}{2}(c_{11}e_{xx}^2 + c_{22}e_{yy}^2 + c_{33}e_{zz}^2) + c_{12}e_{xx}e_{yy} + c_{13}e_{xx}e_{zz}$$
$$+ c_{23}e_{yy}e_{zz} + \frac{1}{2}(c_{44}e_{yz}^2 + c_{55}e_{zx}^2 + c_{66}e_{xy}^2).$$

For a change in the respective vector,

$$e_{xx} = \frac{\delta a}{a}, \quad e_{yy} = \frac{\delta b}{b}, \quad e_{zz} = \frac{\delta c}{c}, \quad e_{yz} = \frac{\delta cb}{b},$$

$$e_{zx} = \frac{\delta ac}{c}, \quad e_{xy} = \frac{\delta ba}{a},$$

where δa is the change in vector a in its own direction, and so forth, while δcb, e.g., means a change in vector c in the direction of b. Now, a deviation from the metastable configuration of κ alumina will result in an increase of the total energy of the crystal. If, e.g., the vector a is changed by an amount δa, in the direction of a, the change of total energy δE will, to leading order, be proportional to the square of δa, and so on. A simultaneous change of the length of all vectors will result in the following change of energy:

$$\delta E = AA \, \delta a^2 + BB \, \delta b^2 + CC \, \delta c^2$$
$$+ AB \, \delta a \, \delta b + AC \, \delta a \, \delta c + BC \, \delta b \, \delta c.$$

The constants AA, BB, CC, AB, AC, and BC are determined in the following way: By changing the length of each vector individually by different amounts, we obtain for each direction a table of energies as a function of the deviation. This table is then least-squares fitted to a function that is parabolic to leading order, and thus the constants AA, BB, and CC are obtained from the curvature. To determine the other constants, the length of two vectors in the unit cell are changed simultaneously. With the previously known constants, a new fit over two variables can be made, say, of the functions x^2, y^2, and xy. This will yield the remaining constants. In a similar manner, for a pure shear, we change a vector in the direction of another. In an obvious notation, the deviation in energy is given by

$$\delta E = A \, \delta cb^2 + B \, \delta ac^2 + C \, \delta ba^2$$

and the constants A, B, and C can be determined by a quadratic fit in one variable. So now we have $\delta U = \delta E / V$. The total-energy calculations are for one unit cell, so $V = abc$. Equating our parabolic fits to the expression for δU, and identifying coefficients, we finally obtain

$$c_{11} = 2AA \frac{a}{bc}, \quad c_{22} = 2BB \frac{b}{ac}, \quad c_{33} = 2CC \frac{c}{ab},$$

$$c_{12} = \frac{AB}{c}, \quad c_{13} = \frac{AC}{b}, \quad c_{23} = \frac{BC}{a},$$

$$c_{44} = 2A \frac{b}{ac}, \quad c_{55} = 2B \frac{c}{ab}, \quad c_{66} = 2C \frac{a}{bc}.$$

For polycrystalline samples it is not possible to calculate the individual elastic constants c_{ij}, but one can measure polycrystalline bulk modulus and shear modulus. In the literature there are several schemes for averaging the elastic constants and sound velocities. For the comfort of the reader, we provide here a quick review of these schemes, and also of the definition of some of the physical quantities later presented.

Voigt[47] has proposed that the averaging of the relations expressing the stress in a single crystal in terms of strain should be made over all possible lattice orientations. Reuss[48] has proposed the averaging of the relations expressing the strain in terms of the given stress.

According to the Voigt[47] approximation, there is a simple relation between the isotropic shear and bulk moduli of a polycrystalline aggregate and the single-crystal elastic constants, c_{ij}:

$$B_V = f_1(c_{ij}), \quad G_V = f_2(c_{ij}). \tag{3}$$

The above equations can be expanded as follows:

$$B_V = \frac{1}{9}(c_{11} + c_{22} + c_{33}) + \frac{2}{9}(c_{12} + c_{13} + c_{23}), \tag{4}$$

$$G_V = \frac{1}{15}(c_{11} + c_{22} + c_{33} - c_{12} - c_{13} - c_{23}) + \frac{1}{5}(c_{44} + c_{55} + c_{66}). \tag{5}$$

Reuss[48] has derived a linear relation between the isotropic shear and bulk moduli of a polycrystalline aggregate and the corresponding single-crystal elastic constants, s_{ij} (the compliances):

$$B_R = f_3(s_{ij}), \quad G_R = f_4(s_{ij}). \tag{6}$$

The above equations can be expanded as follows:

$$B_R = \frac{1}{(s_{11} + s_{22} + s_{33}) + 2(s_{12} + s_{13} + s_{23})}, \tag{7}$$

$$G_R$$
$$= \frac{15}{4(s_{11} + s_{22} + s_{33}) - 4(s_{12} + s_{13} + s_{23}) + 3(s_{44} + s_{55} + s_{66})}. \tag{8}$$

Hill[49] has proved that the Voigt and Reuss equations represent upper and lower limits of the true polycrystalline constants, and he has shown that the polycrystalline moduli are the arithmetic mean values of the Voigt and Reuss moduli and thus given by

$$G_H = \frac{1}{2}(G_R + G_V), \quad B_H = \frac{1}{2}(B_R + B_V). \tag{9}$$

Now definitions follow of some other useful physical quantities, that describe the mechanical properties of a material, and which will later be presented for the aluminas.

The longitudinal modulus can be written as

$$M_H = B_H + \frac{4}{3}G_H. \tag{10}$$

Young's modulus E can be calculated using Hill's shear (G) and bulk (B) moduli, given by the following equation

$$E = \frac{9BG}{3B + G}. \tag{11}$$

Similarly the Poisson's ratio can be defined, using Hill's limits, by the following equation

$$\nu = \frac{3B - 2G}{2(3K + G)}. \tag{12}$$

The probable values of the average shear and longitudinal sound velocities can be calculated from Hill's equations as follows:

$$\nu_s = \sqrt{\left(\frac{G_H}{\rho}\right)}, \quad \nu_l = \sqrt{(B_H + \tfrac{4}{3}G_H)/\rho}. \tag{13}$$

The averaged sound velocity can be computed using the two equations above and can be defined as

$$\nu_m = \left[\frac{1}{3}\left(\frac{2}{\nu_s^3} + \frac{1}{\nu_l^3}\right)\right]^{-1/3}. \tag{14}$$

The Debye temperature θ, which is proportional to the sound velocity, can be calculated by the equation[50]

$$\theta_D = \frac{h}{k}\left[\frac{3n}{4\pi}\left(\frac{N_A\rho}{M}\right)\right]^{1/3}\nu_m, \tag{15}$$

where h is the Planck's constant, k the Boltzmann's constant, N_A Avogadro's number, ρ the density, M the molecular weight, and n is the number of atoms in the molecule.

III. RESULTS

A. Electronic structure and band gaps

The electronic structure has been calculated with both the PWPP+GGA and FPLMTO methods for α- and κ-Al$_2$O$_3$. In this section a general characterization of the results is given. For the α phase there are experimental results available for several quantities, while such are absent for κ-Al$_2$O$_3$. In this way a comparison of theoretical and experimental results for α-Al$_2$O$_3$ serves to give an indication of the accuracy of our predictions for the κ phase.

Figure 2 shows the calculated PWPP total density of states for the α phase. The electronic states below the Fermi level are dominated by O-2p states. The corresponding upper valence-band (UVB) density of states (DOS) peak is about 7.2 eV wide and separated by a huge gap of about 8 eV from the O-2s states, which have a DOS peak width of about 3 eV.

For the α phase, soft-x-ray and photon-energy-spectrum measurements show a UVB width of 9.2–9.5 eV,[51] polarized x-ray emission experiments show one around 8 eV,[52] and x-ray-photoemission measurements show one around 15 eV.[53] The higher experimental values for the UVB width, cf. to the calculated 7.2 eV, can be due to broadening processes present in the experiment. The width of the lower valence-band (LVB) O-2s DOS peak is calculated to be 3 eV, located at around -16 to -19 eV from the top of the valence band. In the x-ray photoemission experiment this width is 6 eV.[53] This LVB difference may be due to correlation effects in these deep-lying semicore-like states, not accounted for in the LDA. The bottom of the conduction band (CB), i.e., the peak around 10 eV, mainly consists of Al-3s states, and the peak around 15 eV comes from the antibonding O-2p and Al-3p states. The CB also has a fair amount of contribution from Al-3d states.

(a)

(b)
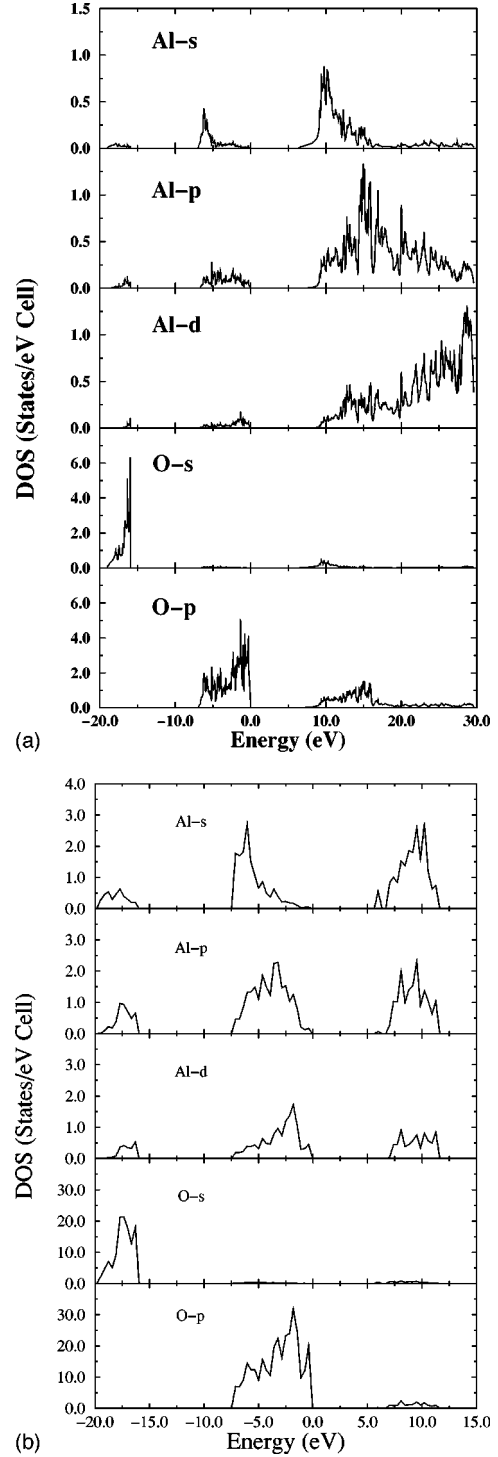
FIG. 2. Calculated density of states (DOS) for Al$_2$O$_3$ in (a) α phase and (b) κ phase (Ref. 6) at experimental volume.

The energy-band structure calculated for the α phase is shown in Fig. 3. There is a direct band gap of 6.6 eV (Ref. 54) at the Γ point. The experimental band gap is 8.8 eV.[1] This type of underestimate is a well-known feature of DFT, mainly when applied to semiconductors and insulators, which occurs because one is wrongly interpreting the true unoccupied states of the system with the corresponding Kohn-Sham states of DFT.[55] The top of the valence band is very flat, which suggests a very large effective hole mass. This is also an indication of the strong bond between the

(a)

(b)
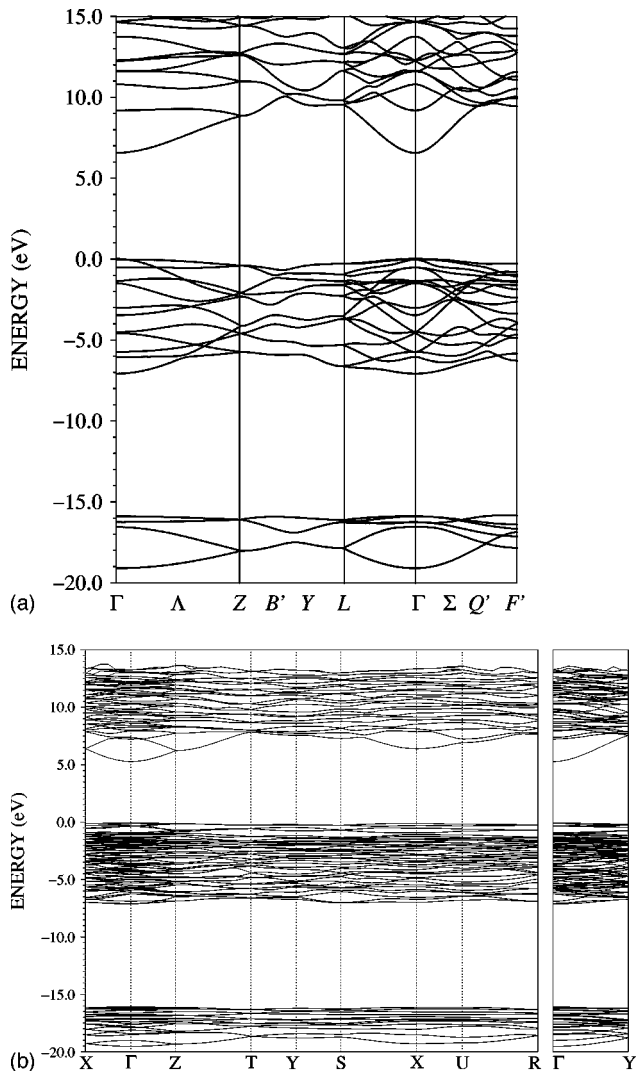
FIG. 3. Calculated energy band structure of Al_2O_3 in (a) α phase and (b) κ phase (Ref. 6) at the equilibrium volume along the major symmetry directions.

corresponding electrons and the host atom. The calculated average effective mass of the conduction band at the Γ point is around 0.4 electron masses. Our effective mass supports the measurements of transport properties by Wills *et al.*,[56] which suggest that the dominating charge carriers are electrons.

In the case of the κ phase, the O-2p and O-2s states are 8.3 and 4.3 eV wide, respectively, and separated by a gap of 8.2 eV. The peak in the LVB DOS is situated at around -16 to -20 eV from the top of the valence band. There is a direct band gap of 5.4 eV for the κ phase at the Γ point.[6]

In short, α- and κ-Al_2O_3 have rather similar electronic structures. The major differences—in addition to those imposed by the difference in atomic structure—are that κ-Al_2O_3 has slightly broader energy bands, a wider energy gap between the upper and lower valence bands, and a narrower band gap, i.e., bridging at the Fermi level. The overall agreement between experiment and theory for α-Al_2O_3 makes the predictions at large for κ-Al_2O_3 likely to apply also in reality.
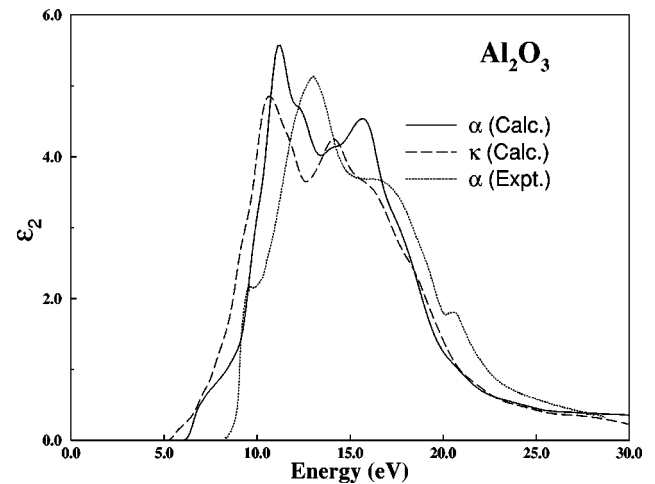
FIG. 4. Calculated (solid) and experimental (Ref. 16) (dotted) imaginary part of the dielectric function, ϵ_2 for α-Al_2O_3 and the calculated one (dashed) for the κ phase.

B. Optical properties

From the electronic structure, optical properties of both α- and κ-Al_2O_3 have been calculated with the FPLMTO method. For the α phase, there are experimental results for several optical quantities given by Arakawa and Williams,[16] while such are absent in the κ phase. Hence, a comparison of theoretical and experimental results for α-Al_2O_3 serves to give an indication of the accuracy of our predictions for the κ phase.

Figures 4 and 5 show the imaginary and real parts of the dielectric functions of the α and κ phases, $\epsilon_2(\omega)$ and $\epsilon_1(\omega)$, respectively. For the α phase our calculated $\epsilon_2(\omega)$ shows two main peaks at around 11 and 15.5 eV and two weak shoulders at around 12.5 and 14 eV; whereas for the κ phase, it has two main peaks at around 10 and 14 eV and one weak shoulder around 15.5 eV. The experimental data[16] for α-Al_2O_3 show interband transitions at 13, 16.5, and 20.5 eV. The latter small structure is absent in our calculated ϵ_2, where we just see a smooth variation in this energy range. For the first two main peaks there is a constant difference between the calculated and experimental positions, mainly
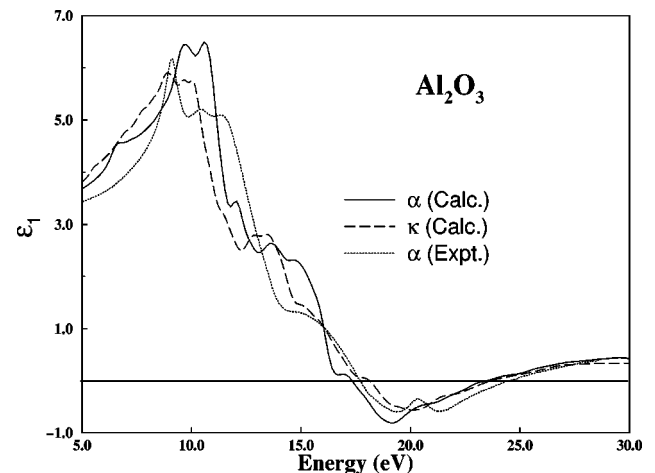
FIG. 5. Calculated (solid) and experimental (Ref. 16) (dotted) real part of the dielectric function ϵ_1 for α-Al_2O_3 and the calculated one (dashed) for the κ phase.
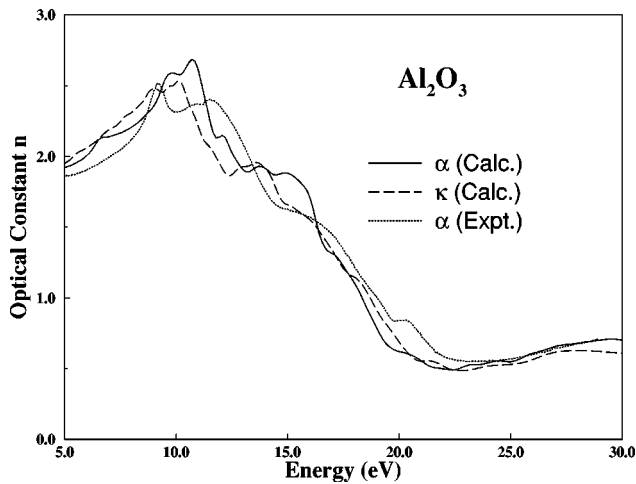
FIG. 6. Calculated (solid) and experimental (Ref. 16) (dotted) optical constant n for α-Al$_2$O$_3$ and the calculated one (dashed) for the κ phase.

FIG. 7. Calculated (solid) and experimental (Ref. 16) (dotted) optical constant k for α-Al$_2$O$_3$ and the calculated one (dashed) for the κ phase.

because our band gap is smaller than the experimental one by approximately 2 eV. If we shift the calculated curve by 2.0 eV, the calculated spectrum would be in better agreement with experiment. However, the steep slope near the absorption edge and the sharp peak, both present in the experimental spectrum, are absent in the calculated one. This excitonic peak is naturally missing in our calculated spectra, because they only involve interband transitions from valence- to conduction-band states.

The behavior of the $\epsilon_2(\omega)$ curve for κ-Al$_2$O$_3$, in general, agrees with that of the α phase. However, the rigid shift is about 3.0 eV.

The origins of the different peaks in the calculated dielectric functions can be deduced in terms of interband transitions. According to selection rules, only such transitions are allowed that imply a change of the angular momentum quantum number l by 1, i.e., $\Delta l = \pm 1$. For α-Al$_2$O$_3$ the first peak at around 11 eV in the calculated spectrum can be assigned to transitions from Al-$3p$ to Al-$3s$ states. Transitions from Al $3d$ to Al $3p$ may give rise to the second main peak around 15.5 eV.

The real part of the dielectric function ϵ_1 is given by a Kramers-Kronig analysis of ϵ_2. In Fig. 5 the calculated ϵ_1 of both phases are compared to experimental data of the α phase. As one can see, most features of the measured data are well reproduced by our calculations. The calculated ϵ_1 curves for the α and κ phases become negative at 17.3 and 18.2 eV, and both become positive again at 23.6 eV, the corresponding experimental values for the α phase being 17.7 and 24.5 eV, respectively. In the high-energy region, the calculated and measured ϵ_1 curves show very similar behavior. On the other end of the spectrum, the dielectric function $\epsilon_1(0)$ is calculated to be 3.2 for both the α and κ phases, whereas the experimental α-Al$_2$O$_3$ result is 3.1,[13] hence showing very good agreement. The calculation of Ching and Xu[17] gives a value of 3.86, in worse agreement than our FPLMTO value.

The calculated optical constants n and k are shown in Figs. 6 and 7 together with the experimental data of Arakawa and Williams. Our calculated values of the ordinary refractive indexes for the α and κ phases are both 1.79, while the
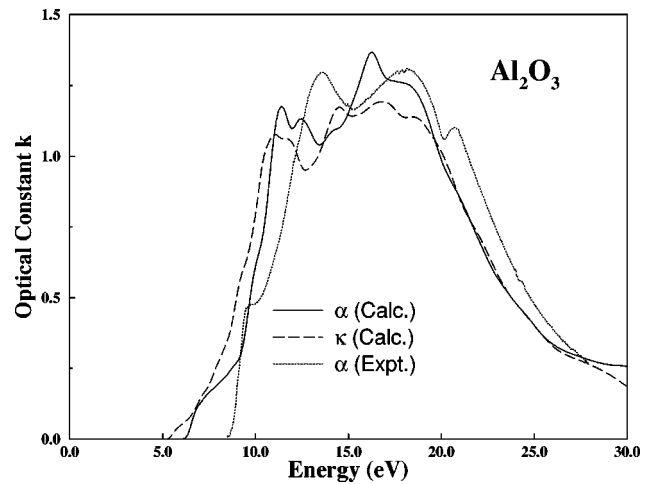
measured values by Zouboulis and Grimsditch is 1.774 for the α phase. The calculated value of the ordinary refractive index by Ching and Xu[17] using the OLCAO method is 1.96. Our present theoretical result for the refractive index is in excellent agreement with experiment. In passing, we point out here that we do not agree with the argument of Ching and Xu, who claim that the difference in their calculated and experimental values is due to the excitonic effects that are not included in the theory. Our calculated spectra in Figs. 6 and 7 show a good general agreement with experiment, although there is some discrepancy regarding the peak positions, mainly, as already mentioned, originating in the shortcomings that follow when describing the conduction regime of the band structure with DFT.

We have also calculated the optical reflectivity conductivity. We have compared these with the recent experimental data of Bortz and French.[15] In Fig. 8 we show the reflectivity spectrum. The measured spectrum shows an excitonic peak at 9.1 eV, which is not present in our calculations. However, the other features of the experimental spectrum, at 12.0, 12.9, 14.9, 17.4, and 21.8 eV, are well represented in our
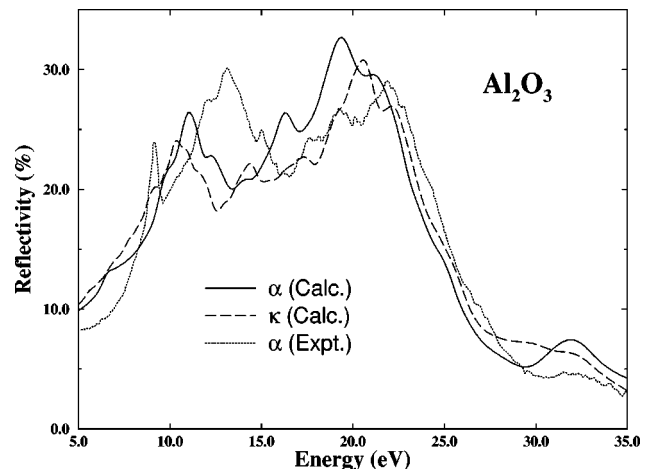
FIG. 8. Calculated (solid) and experimental (Ref. 15) (dotted) reflectivity (%) for α-Al$_2$O$_3$ and the calculated one (dashed) for the κ phase.
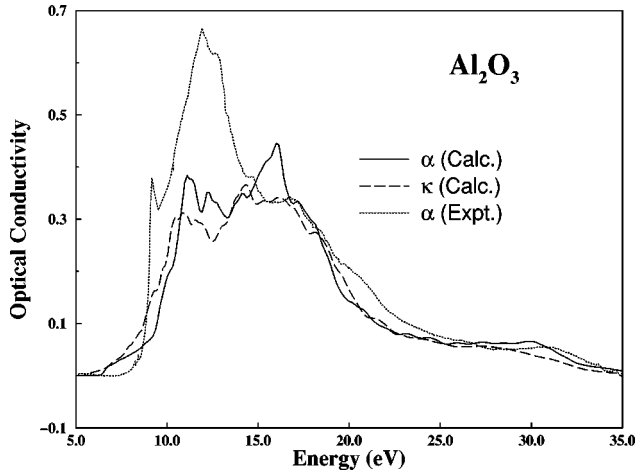
FIG. 9. Calculated (solid) and experimental (Ref. 15) (dotted) conductivity (arb. units) for α-Al$_2$O$_3$ and the calculated one (dashed) for the κ phase.

calculations, which show features at 11.3, 12.5, 14.4, 16.6, 19.5, and 22.0 eV, respectively. Bortz and French also observed a peak at 32 eV, as do we in our calculations. This last peak arises from interband transitions from the LVB O-2s states to the antibonding O-2p states. Observe that the calculated positions of the features are very similar for both phases.

The calculated and experimental optical conductivities are plotted in Fig. 9. The measured conductivity is generally higher than the calculated one. Our calculations show two main peaks, and features at 11.5, 12.4, 14.5, 16.5, 17.4, and 30.5 eV, again for both phases. The measured spectrum shows an excitonic feature at 9.1 eV and other features at 12.4, 13.2, 14.5, 17.4, and 31.5 eV. Thus, apart from features resulting from many-body effects (excitons, etc.), good agreement between the calculated and measured spectra has been obtained. Further, the similarity of the last few physical
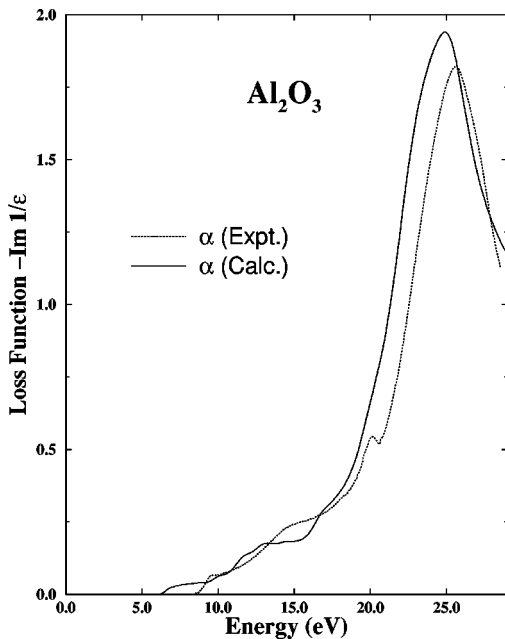
FIG. 10. Calculated (solid) and experimental (Ref. 16) (dotted) energy loss function (arb. units), $-$ Im 1/ϵ for α-Al$_2$O$_3$.

TABLE I. Comparison between the experimental and theoretical crystallographic lattice parameters for Al$_2$O$_3$.

	Expt.		Calc.	
	κ^a	α^b	κ	α
V (Å^3)	359.10	255.04	352.07,^{c} 351.2^d	255.1,^{e} 253,^{d} 255^e
b/a	1.7189	1.0	1.7182	1.0
c/a	1.8482	2.73	1.8481	2.731,^{c} 2.73,^{d} 2.721^e
B (GPa)		254.4	251.8,^{c} 246.7^d	244.0,^{c} 253.5,^{d} 243.8^e

[a]Reference 65.
[b]Reference 64.
[c]PWPP.
[d]FPLMTO.
[e]LCGTOFF.

properties calculated for the two phases investigated indicates their similarity as far as optical properties are concerned.

In Fig. 10, we have plotted the energy-loss function $-$ Im(ϵ)$^{-1}$ for the α phase. This function is proportional to the probability that fast electrons traversing the bulk material will lose energy. For a free-electron gas, with $\epsilon_2 \sim 0$, $-$ Im(ϵ)$^{-1}$ has a maximum at the plasma energy E_p given by

$$E_p = \frac{h}{2\pi}\left[\left(\frac{4\pi Nne^2}{m_{\text{eff}}}\right)\right]^{1/2}, \qquad (16)$$

where N is the number of atoms (or molecules) per unit volume, m_{eff} the effective mass of the electrons, and n the number of electrons per atom (or molecule) that would participate in the volume-plasma oscillations induced by fast electrons traversing the material. We can assume m_{eff} to be the free-electron mass, because, in the absence of strong interband transitions in the vicinity of the plasma resonance, the behavior of the valence electrons would be virtually like that of unbound or free electrons that undergo plasma oscillations. Hence, one would expect the peak of $-$ Im(ϵ)$^{-1}$ to be in the vicinity of the plasma energy calculated using the total number of valence electrons. The total number of valence electrons per Al$_2$O$_3$ molecule is 24 and substitution of this number and with m_{eff} equal to the free-electron mass into the above equation yields $E_p = 27.8$ eV. It is seen from Fig. 10 that for Al$_2$O$_3$, $-$ Im(ϵ)$^{-1}$ has its maximum at 25.8 eV from experiment and at 25.0 eV from our calculations, thus showing that our assumptions are reasonable.

TABLE II. Calculated (PWPP) values for the elastic constants c_{ij} for κ-Al$_2$|O$_3$ together with calculated and experimental ones of the α phase.

	Elastic constants (GPa)								
Constants	c_{11}	c_{22}	c_{33}	c_{44}	c_{55}	c_{66}	c_{12}	c_{13}	c_{23}
κ-Al$_2$O$_3$	460	410	450	120	140	160	125	95	145
α-Al$_2$|O$_3$	480		480	140			155	117	
α-Al$_2$O$_3^a$	497		502	147			163	117	

[a]Reference 8.

TABLE III. The isotropic bulk modulus (B in GPa), shear modulus (G in GPa), longitudinal modulus (GPa), Young's modulus (GPa), and Poisson's ratio.

	B_R	B_V	B_H	G_R	G_V	G_H	M_H	E	ν
κ-Al$_2$O$_3$	229.4	227.8	228.6	144.8	147.7	146.3	423.7	361.7	0.24
α-Al$_2$O$_3$	245.7	246.4	246.1	156.8	158.6	157.7	456.4	390	0.24
Expt. (α-Al$_2$O$_3$) [a]	253	255	248	164	165.3	164.7	467.6	404.6	0.23

[a]Reference 8.

C. Elastic properties

In this section we present our results for the elastic properties. Also for these, there exist experimental data for the α phase but none for the κ phase. So the α alumina results serve to give confidence in the methods, while the κ ones are theoretical predictions. We emphasize again that the reason that the elastic constants of κ alumina have not yet been determined experimentally is that this phase only grows in small grains. It is thus hard to obtain pure, isotropic, specimens that are large enough for experimental investigations.

Calculated values for equilibrium volume, axial ratios, and bulk moduli obtained from the EOS for the κ and α phases are presented in Table I. For the α phase we have also included the results from the recent calculations of Boettger[12] and thus demonstrate that three different computational methods give results in mutual agreement and in satisfactory agreement with experiment.[8]

Table II lists calculated values for the elastic constants of the κ and α phases along with experimental data for the α phase. As previously mentioned, six and nine independent elastic constants exist for the α and κ phases, respectively, consistent with their symmetry. In general, our calculated elastic constants for the α phase are lower than the experimental ones by some 4–5 %. In the case of c_{13}, our calculated value agrees exactly with the experimental value.

One can observe that the calculated elastic constants, c_{11}, c_{33}, c_{44}, c_{12}, and c_{13}, of the κ phase are 20–30 GPa lower than the corresponding calculated elastic constants of the α phase. There is one exception, however, namely c_{66} for which the calculated values for both phases are equal.

In order to compare our calculated elastic constants of the α phase with the values from the LCGTOFF calculations[12] and lattice-dynamics (LD) calculations,[57] Table III shows calculated numbers for the four symmetry-preserving elastic constants, $c_{11}+c_{12}$, c_{33}, c_{13}, and c_t, together with experimental data.[8] The tetragonal shear modulus, c^t, can be defined by the following equation

$$c^t = \frac{1}{6}[(c_{11}+c_{12})+2c_{33}-4c_{13}]. \tag{17}$$

There is very close agreement between ours and Boettger's[12] calculated values for these four elastic constants of α-Al$_2$O$_3$ (Table III). His calculated values of elastic constants ($c_{11}+c_{12}$) and c^t, however, are in better agreement with experiment than our present values, while for c_{33} and c_{13} the opposite is true. The deviations from experiment are typically 5% or less, nonetheless. As argued in Ref. 12, this systematic deficiency can again be attributed to the DFT. It is also possible to calculate three other elastic properties that are routinely accessible from EOS measurements.

The static bulk modulus[58] can be calculated by the following equation:

$$B = \frac{c_{33}(c_{11}+c_{12})-2c_{13}^2}{(c_{11}+c_{12})+2c_{33}-4c_{13}}. \tag{18}$$

The pressure derivatives of the hexagonal lattice constants are given by

$$a' = \frac{c_{33}-c_{13}}{2c_{13}^2-c_{33}(c_{11}+c_{12})} \tag{19}$$

and

$$c' = \frac{(c_{11}+c_{12})-2c_{13}}{2c_{13}^2-c_{33}(c_{11}+c_{12})}. \tag{20}$$

As seen in Table IV, our calculated values for the pressure derivatives and Boettger's values are in good mutual and experimental agreement, as are those for the bulk modulus.

In Table V, we present our calculated bulk and shear moduli in the Ruess, Voigt, and Hill approximations for the κ and α phases, together with the longitudinal modulus, Young's modulus, and Possion's ratio within the Hill scheme. Our calculated values for polycrystalline aggregates are lower for the κ phase than for the α phase. In comparison with experimental ones, possible only for the α phase, all our calculated values are within less than 5% off the measured ones.

In Table VI, we have also calculated the Debye temperature for the κ and α phases from our elastic constants. Our calculated sound velocities and Debye temperatures for the α phase are within 2% of the experimental value. The calculated values for the κ phase are lower than for the α phase.

TABLE IV. Theoretical and experimental values for four symmetry-preserving elastic constants of corundum (in GPa).

	($c_{11}+c_{12}$)	c_{33}	c_{13}	c^t
LD[a]	697	455	130	181
LCGTOFF[b]	652.4	478.3	115.4	191.2
PWPP (present)	635	480	117	188
Expt.[c]	660.2	501.8	117.2	199.2
Expt.[d]	660.1	500.9	116.0	199.6

[a]Reference 57.
[b]Reference 12.
[c]Reference 8.
[d]Reference 9.

TABLE V. Theoretical and experimental values for the bulk modulus (B; GPa) and the pressure derivatives of lattice parameters (a' and c'; GPa^{-1}) for α-Al$_2$O$_3$.

	B	a'	c'
PIB (TF)[a]	264	$-0.000\ 89$	$-0.001\ 09$
PIB (KS)[a]	356	$-0.001\ 10$	$-0.001\ 46$
OLCAO[b]	242		
LAPW+LO[c]	257		
LCGTOFF[d]	248.7	$-0.001\ 27$	$-0.001\ 48$
PWPP (present)	246.2	$-0.001\ 31$	$-0.001\ 45$
Expt.[e]	254.4		
Expt.[f]	257	$-0.001\ 22$	$-0.001\ 36$
Expt.[g]	239	$-0.001\ 37$	$-0.001\ 34$

[a]Reference 67.
[b]Reference 17.
[c]Reference 2.
[d]Reference 12.
[e]Reference 64.
[f]Reference 65.
[g]Reference 66.

All these comparisons with experiment for α-alumina suggest that our calculated values for the κ phase should be highly reliable.

In an experimental investigation of the mechanical properties of κ alumina by Söderlund *et al.*,[59] elastic anisotropy has indeed been found, in contrast to the elastic isotropy of α-alumina. The elastic constant in the direction of crystal growth was found to be higher than in perpendicular directions. The direction of growth is parallel to c, and elastic properties along this direction are easier to determine than properties perpendicular to it. In the same investigation it was also found that the elastic constants of κ-Al$_2$O$_3$, as compared to the α phase, are lower mainly in directions perpendicular to c, while along c they are higher. Our theoretical results are in satisfactory agreement with these observations, since we notice that on the average the constants that determine the elastic behavior perpendicular to the c axis (c_{11}, c_{22}, and c_{12}) are lower than the constants describing properties along it (c_{33}, c_{13}, and c_{23}). However, our results indicate a profound elastic anisotropy between the a and b axes, which has yet to be seen experimentally.

IV. CONCLUSIONS

We have presented results for electronic, elastic, and optical properties of the κ and α phases of aluminum oxide with two different electronic structure methods. As far as the κ phase is concerned, our results for the elastic and optical properties are predictions, and we welcome experiments to prove them. For the α phase, our calculations give different results for the elastic constants, confirming the earlier first-principles calculation by Boettger[12] for symmetry-preserving elastic constants and extending the database to nonsymmetry ones. Our calculated values for shear and bulk moduli of polycrystalline α-Al$_2$O$_3$ aggregates are in good agreement with experiment, as are the calculated shear and longitudinal velocities as well as the Debye temperature.

For the α phase, we have also made a detailed comparison between our calculated optical properties and measured spectra from two different experiments. Our calculated values for the ordinary refractive index and static dielectric

TABLE VI. The density (ρ in g/cm^3), shear, longitudinal, and mean sound velocity (ν_l, ν_s, ν_m in 10^5 cm/s) and the Debye temperature (θ) obtained from the mean sound velocity (θ in K).

	ρ	ν_l	ν_s	ν_m	θ
κ-Al$_2$O$_3$	3.870	10.48	6.16	6.83	997
α-Al$_2$O$_3$	3.984	10.72	6.30	6.98	1029
Expt.[a] (κ-Al$_2$O$_3$)	3.786				
Expt.[b] (α-Al$_2$O$_3$)	3.985	10.84	6.44	7.13	1051

[a]Reference 63.
[b]Reference 8.

functions are in better agreement with experiment than the earlier calculation of Ching and Xu.[17] However, the remaining discrepancy between the calculated and experimental dielectric functions is somewhat unsatisfactory. A remedy for this would be to take excitonic effects into consideration.[60]

To give an account for our conclusions of the consequences of the phase transition between α and κ alumina, we note the following.

Optical properties seem to be virtually unaffected, this being indicated by our reported similarity between the relevant quantities for the two phases. Elastic properties and other virtues that depend on lattice dynamics, on the other hand, are significantly altered, generally becoming lower in magnitude in the κ phase and showing anisotropy.

The interesting fact that the band gap of the κ phase is ~ 1 eV lower in our LDA calculations deserves special attention. This question needs to be further investigated, as, in general, a DFT calculation does not reproduce the band gap correctly. However, following intuition, this error should be systematic, and if this is the case, κ alumina, because of its smaller band gap, could show good conductivity or semiconductivity at elevated temperatures. This phenomenon has already been detected in the α phase[1] and is due to the reduction of the band gap with temperature, partly because of lattice expansion, partly because the electrons couple to vibrational modes. To resolve this question, a many-body calculation, e.g., invoking a GW correction,[61] should be performed for both phases. Such a calculation has already been performed for an oxide, Li$_2$O.[62] However, Li$_2$O has a unit cell containing 3 atoms, whereas the one of α-Al$_2$O$_3$ has 10 and the one of κ 40. So further theoretical investigation, and extensive computer power, will be necessary.

In summary, electronic, elastic, and optical properties of the κ and α phases of aluminum oxide have been calculated with two different electron structure methods. A number of comparisons with experimental results for α-alumina suggest that our calculated results for the κ phase should have high predictive value. For ground-state and mechanical properties, the results following from the PWPP method are as good as those from the more time consuming FPLMTO method.

ACKNOWLEDGMENTS

[1] R. H. French, J. Am. Ceram. Soc. **73**, 477 (1990).

[2] F. C. Marton and R. E. Cohen, Am. Mineral. **79**, 789 (1994).

[3] M. V. Finnis, J. Phys.: Condens. Matter **8**, 5811 (1996).

[4] C. Verdozzi, D. R. Jennison, P. A. Schultz, M. P. Sears, J. C. Barbour, and B. G. Potter, Phys. Rev. Lett. **80**, 5615 (1998).

[5] B. Ollivier, R. Retoux, P. Lacorre, D. Massiot, and G. Ferey, J. Mater. Chem. **7**, 1049 (1997).

[6] Y. Yourdshayan *et al.* (to be published).

[7] R. W. G. Wyckoff, *Crystal Structures*, 2nd ed. (Wiley, New York, 1964).

[8] J. H. Gieske and G. R. Barsch, Phys. Status Solidi **29**, 121 (1968).

[9] W. E. Tefft, J. Res. Natl. Bur. Stand., Sect. A **70A**, 277 (1966).

[10] T. Goto, O. L. Anderson, I. Ohno, and S. Yamamoto, J. Geophys. Res. **94**, 7588 (1989).

[11] E. S. Zouboulis and M. Grimsditch, J. Appl. Phys. **70**, 772 (1991).

[12] J. C. Boettger, Phys. Rev. B **55**, 750 (1997).

[13] A. K. Harman, S. Ninomiya, and S. Adachi, J. Appl. Phys. **76**, 8032 (1994).

[14] T. Tomiki, Y. Ganaha, T. Futemma, T. Shikenbaru, Y. Aiura, M. Yuri, S. Sato, J. Fukutani, H. Kato, T. Miyahara, J. Tamoshiro, and A. Yonesu, J. Phys. Soc. Jpn. **62**, 1372 (1993).

[15] M. L. Bortz and R. H. French, Appl. Phys. Lett. **55**, 1955 (1989).

[16] E. T. Arakawa and M. W. Williams, J. Phys. Chem. Solids **29**, 735 (1968).

[17] W. Y. Ching and Y-N. Xu, J. Am. Ceram. Soc. **77**, 404 (1994).

[18] M. C. Payne, M. P. Teter, D. C. Allan, T. A. Arias, and J. D. Joannopoulos, Rev. Mod. Phys. **64**, 1045 (1992).

[19] J. M. Wills (unpublished); J. M. Wills and B. R. Copper, Phys. Rev. B **36**, 3809 (1987).

[20] M. Fuchs and M. Scheffler (unpublished).

[21] P. Hohenberg and W. Kohn, Phys. Rev. **136**, B864 (1964).

[22] W. Kohn and L. J. Sham, Phys. Rev. **140**, A1133 (1965).

[23] O. Gunnarsson and B. I. Lundqvist, Phys. Rev. B **13**, 4274 (1976).

[24] R. O. Jones and O. Gunnarsson, Rev. Mod. Phys. **61**, 689 (1989).

[25] R. M. Dreizler and E. K. U. Gross, *Density Functional Theory—An Approach to the Quantum Many-Body Problem* (Springer-Verlag, Berlin, 1990).

[26] B. Hammer, K. W. Jacobsen, V. Milman, and M. C. Payne, J. Phys.: Condens. Matter **4**, 10 453 (1992).

[27] N. Troullier and J. L. Martins, Phys. Rev. B **43**, 1993 (1991).

[28] G. B. Bachelet, D. R. Hamann, and M. Schlüter, Phys. Rev. B **26**, 4199 (1982).

[29] M. Gillan, J. Phys.: Condens. Matter **1**, 689 (1989).

[30] H. J. Monkhorst and J. D. Pack, Phys. Rev. B **13**, 5188 (1976).

[31] Y. Yourdshahyan, C. Ruberto, L. Bengtsson, and B. I. Lundqvist, Phys. Rev. B **56**, 8553 (1997).

[32] D. M. Ceperley and B. J. Alder, Phys. Rev. Lett. **45**, 566 (1980).

[33] J. P. Perdew and A. Zunger, Phys. Rev. B **23**, 5048 (1981).

[34] J. P. Perdew, J. A. Chevary, S. H. Vosko, K. A. Jackson, M. R. Pederson, D. J. Singh, and C. Fiolhais, Phys. Rev. B **46**, 6671 (1992).

[35] B. Hammer, K. W. Jacobsen, and J. K. Norskov, Phys. Rev. Lett. **70**, 3971 (1993).

[36] L. Hedin and B. I. Lundqvist, J. Phys. C **4**, 2064 (1971).

[37] O. K. Andersen, Phys. Rev. B **12**, 3060 (1975).

[38] H. L. Skriver, *The LMTO Method* (Springer, Berlin, 1984).

[39] A good description of the calculation of dielectric constants and related properties are found in T. Gashe, thesis, Uppsala University, 1993.

[40] A. R. Edmonds, *Angular Momentum in Quantum Mechanics* (Princeton University Press, Princeton, NJ, 1974), p. 82.

[41] In practice we calculate matrix elements of the symmetrized momentum operator $\langle i | \vec{\mathbf{p}}_\mu | j \rangle \equiv [\langle i | p_\mu j \rangle + (-1)^\mu \langle p_{-\mu} i | j \rangle]/2$.

[42] M. A. Khan, J. Phys. Soc. Jpn. **62**, 1682 (1993); Appl. Surf. Sci. **65**, 18 (1993).

[43] P. M. Oppeneer, T. Maurer, J. Sticht, and J. Kübler, Phys. Rev. B **45**, 10 924 (1992).

[44] R. Ahuja, O. Eriksson, B. Johansson, S. Auluck, and J. M. Wills, Phys. Rev. B **54**, 10 419 (1996).

[45] Y. Yourdshahyan, U. Engberg, L. Bengtsson, B. I. Lundqvist, and B. Hammer, Phys. Rev. B **55**, 8721 (1997).

[46] B. B. Karki, M. C. Warren, L. Stixrude, G. J. Ackland, and J. Crain, Phys. Rev. B **55**, 3465 (1997).

[47] W. Voigt, *Lehrbuch der Kristallphysik* (Taubner, Leipzig, 1928).

[48] A. Reuss, Z. Angew. Math. Mech. **9**, 55 (1929).

[49] R. Hill, Proc. Phys. Soc. London, Sect. A **65**, 350 (1952).

[50] O. L. Anderson, J. Phys. Chem. Solids **24**, 909 (1963).

[51] W. L. O'Brien, J. Jia, Q-Y. Dong, T. A. Callcott, D. R. Mueller, D. L. Ederer, and C-C. Kao, Phys. Rev. B **47**, 140 (1993).

[52] G. Dräger and J. A. Leiro, Phys. Rev. B **41**, 12 919 (1990).

[53] A. Balzarotti and A. Bianconi, Phys. Status Solidi B **76**, 689 (1976).

[54] Literature gives 6.2–6.6 eV depending on the method used.

[55] *Theory of the Inhomogeneous Electron Gas*, edited by S. Lundqvist and N. H. March (Plenum, New York, 1983), and references therein.

[56] F. G. Wills, H. G. deLorenzi, and K. H. Janora, J. Am. Ceram. Soc. **75**, 2709 (1992).

[57] R. E. Cohen, Geophys. Res. Lett. **12**, 725 (1985).

[58] H. J. F. Jansen and A. J. Freeman, Phys. Rev. B **35**, 8207 (1987).

[59] E. Söderlund, I. Reineck, and D. J. Rowcliffe, J. Mater. Res. **9**, 1683 (1994).

[60] L. X. Benedict, E. L. Shirley, and R. B. Bohn, Phys. Rev. Lett. **80**, 4514 (1998).

[61] L. Hedin, Phys. Rev. A **139**, 796 (1965).

[62] S. Albrecht, G. Onida, and L. Reining, Phys. Rev. B **55**, 10 278 (1997).

[63] M. Halvarsson, V. Langer, and S. Vuorinen, Surf. Coat. Technol. **76-77**, 287 (1995).

[64] H. d'Amour, D. Schiferl, W. Denner, H. Schulz, and W. B. Holzapfel, J. Appl. Phys. **49**, 4411 (1978).

[65] Y. Sato and S. Akimoto, J. Appl. Phys. **50**, 5285 (1979).

[66] J. Xu, High Temp.-High Press. **19**, 661 (1987).

[67] H. Cynn, D. G. Isaak, R. E. Cohen, M. F. Nicol, and O. L. Anderson, Am. Mineral. **75**, 439 (1990).